

# We are IntechOpen, the world's leading publisher of Open Access books Built by scientists, for scientists

6,900

Open access books available

186,000

International authors and editors

200M

Downloads

Our authors are among the

154

Countries delivered to

TOP 1%

most cited scientists

12.2%

Contributors from top 500 universities



WEB OF SCIENCE™

Selection of our books indexed in the Book Citation Index  
in Web of Science™ Core Collection (BKCI)

Interested in publishing with us?  
Contact [book.department@intechopen.com](mailto:book.department@intechopen.com)

Numbers displayed above are based on latest data collected.  
For more information visit [www.intechopen.com](http://www.intechopen.com)



# Experimental Study of Local Scour around Side-by-Side Bridge Piers under Ice-Covered Flow Conditions

*Mohammad Reza Namaee, Jueyi Sui and Peng Wu*

## Abstract

A precise prediction of maximum scour depth (MSD) around piers under ice-covered conditions is crucial for the safe design of the bridge foundation. Due to the lack of information for local scour under ice-covered flow condition, it is extremely hard to give proper estimation of MSD. In the current study, a set of flume experiments were completed to investigate local scour around four pairs of circular bridge piers with nonuniform bed materials under open channel, smooth and rough ice cover conditions. Three different bed materials with median particle size of 0.47, 0.50, and 0.58 mm were used to simulate natural river conditions. Regardless of pier size, the maximum scour depths were observed in front of the piers under all flow conditions. Additionally, a smaller pier size and a larger space between piers yield a smaller scour depth. Results showed that the maximum scour depth decreases with increase in the grain size of armor layer. The distribution of vertical velocity shows that the strength of downfall velocity is the greatest under rough ice cover. Empirical equations were developed to estimate the maximum scour depth around side-by-side bridge piers under both open-channel and ice-covered flow conditions.

**Keywords:** ice cover, local scour, nonuniform sand, bridge piers, maximum scour depth

## 1. Introduction

### 1.1 Water and sediment motion around hydraulic structures

The flow of water with sediment content is important for hydraulic engineers involved with water supply and flood control projects. Considered as a two-phase flow, water and sediment motion is described as an energy-coupled process, resulting in erosion and scour, suspension, transport, advection, dispersion, and deposition of sediment [1]. Mechanics of sediment transport is important for the design of hydraulic structures in the following aspects:

- General scour of an alluvial river
- Local scour at a hydraulic structure, such as at bridge piers and abutments

- Deposition of sediment in flow zones where the existing sediment concentration exceeds the sediment transport capacity of the stream

Generally speaking, alluvial riverbeds are likely to experience continuous changes over time. In one case, flowing water erodes, moves, and gradually collects sediment in the river, modifying its bed elevation and slightly changing its boundaries. Changes in bed elevation could be resulted from either natural process (general scour) or human activities which lead to alteration of the riverbed or river geometry [2]. Placement of bridge piers inside the river is one of the most common engineering practices in which the bridge pier is in direct contact with the flowing water. The main issue associated with the interaction of flowing water and the bridge pier is the scouring process which occurs around the bridge piers and is known as local scour. Depending on the intensity of approaching flow for sediment transport, local scour process around bridge piers is classified as either clear-water scour or live-bed scour. Clear-water scour occurs when there is no movement of the bed material from the upstream flow, while live-bed scour occurs when the scour hole is consistently supplied with sediments by the upstream flow [3]. Due to local scour, the flow pattern around the pile foundation will be changed, which ultimately leads to the creation of horseshoe vortex in front of the pier, the wake vortex behind the pier, and the contraction of streamlines at the side edges of the pile [4]. The horseshoe vortex is created by the flow of water separating at the upstream face of the bridge pier where the initial scour hole has developed. Wake vortices develop behind a bridge pier and disturb the downstream flow pattern [5]. These vortices are the main causes of local scour creation, and they lead to an intensification in the local sediment transport capacity and the expansion of local scour around the pile foundation or currents in marine environment. Due to local scour, the insertion depth of the pile reduces as the scour depth around the pile grows, which is directly associated with the stability of pile foundation. The deeper the depth of local scour around the pile, the more vulnerable pile foundation becomes which leads to bridge collapse in the most extreme case [4]. Therefore, it is commonly accepted that local scour is one of the main causes of pile foundation failure in marine environments. Briand and Hunt [6] declared that 1502 bridges failed due to bridge scour in the United States between 1966 and 2005. Wardhana and Hadipriono [7] also did their research on 500 cases of bridge structure collapse in the United States between 1989 and 2000 and specified that the most common reason for bridge collapse was scour and floods. Therefore, estimation and identification of variations in bed level in the vicinity of bridge piers are crucial for their safe design. The development of local scour hole around bridge piers is jointly associated with the characteristics of flow pattern near the bed and around the pier. The characteristics of flow pattern around the vertical circular piers are clearly fully three-dimensional (3D) and complex. The tremendous complexity of three-dimensional flow field around a pier is attributed to separation and generation of multiple vortices. It is even more aggravated because of the dynamic interaction between the flow and the movable bed throughout the development of a scour hole (see [8]).

## **1.2 The impact of ice cover on the maximum scour depth (MSD)**

The precise prediction of scour patterns around bridge piers depends on recognition of the flow field and the mechanism of sediment transport in and out of the scour hole [9]. Turbulence and the induced secondary flow field around the bridge element have been studied comprehensively in the last decades both experimentally (e.g., [5, 10, 11]) and numerically (e.g., [12, 13]). Many hydraulic researchers have done experiments to investigate the local scour around bridge

piers and developed empirical equations to estimate the maximum scour depth [5, 14–18]. However, most of them were focused on local scour around singular bridge piers, while multiple pile bridge piers have become more common in recent years in bridge design for geotechnical and economic reasons. These types of pier can significantly reduce construction costs with a higher efficiency [19], though the nature of the scour development in the vicinity of bridge pier groups is more complex than single bridge pier case. Hannah declared that the maximum scour depth around side-by-side piers is approximately 50% more than that around a single pier if the pier spacing ratio is 0.25 [20]. Salim and Jones [21] observed that the scour depth decreases as the spacing between the piles increases.

The most extreme cases of local scour around bridge piers occur in cold regions where the surface of flow is covered by ice. The influence of ice cover on a channel involves in complex interactions among the ice cover, fluid flow, and channel geometry. This complex interaction can have a dramatic effect on the sediment transport process [22]. The ice cover presence increases the complexity of hydraulic processes in rivers and sometimes extremely influences river characteristics such as hydrodynamics and morphology [23]. When ice floes move discretely and freely (e.g., in the case of low surface concentrations of ice pans during freeze-up), the ice resistance effect is slight, and water levels do not modify greatly [24]. In practice, ice cover appears quite often in rivers in the cold regions during the winter. The presence of an ice cover increases the wetted perimeter by adding an additional boundary to the water surface. Under ice-covered flow conditions, the flow is highly sensitive to the friction parameter [25]. The existing number of research on local scour around bridge pier under ice-covered rivers is very limited, due to the difficulties in obtaining field data from ice-covered rivers. Ackermann et al. [26] did a laboratory investigation on the effect of ice cover on local scour around circular bridge piers. The results showed that for equivalent averaged flow velocities, the existence of an ice cover could increase the local scour depth by 25–35% from the free surface condition. Bacuta and Dargahi [27] carried out laboratory tests in a flume with a simulated ice cover for clear-water conditions. They found that the extent of scour is larger for ice-covered flows. Wu et al. [28] studied the effect of relative bed coarseness, flow shallowness, and pier Froude number on local scour around a bridge pier and reported that the scour depth under covered conditions is larger than that under open-channel flow conditions.

*Objectives:* The first objective of this study is to investigate the impact of bridge spacing on the maximum scour depths around multiple bridge piers under open-channel and ice-covered flow conditions.

### **1.3 The velocity distribution under ice-covered flow conditions**

The appearance of an ice cover in river changes the velocity profile [29]. Under ice-covered flow condition, the upper portion of the flow is mainly affected by the ice cover resistance, while the lower portion of flow is primarily influenced by the channel bed resistance [29]. The maximum flow velocity under ice cover is located somewhere between the channel bed and ice cover depending on the ratio of the ice resistance coefficient to the bed resistance coefficient [30]. According to Wang et al. [24], it is expected that as the ice resistance increases, the maximum flow velocity will move closer to the channel bed. In terms of transverse flow distributions and velocities of secondary currents, ice cover can impact flows in an existing thalweg, altering the position of the thalweg and changing the morphology of the stream which in an extreme case will lead to bank and bed erosion [31]. Due to the difficulty of making velocity measurements under ice-covered conditions, nearly all

the studies regarding velocity distribution around bridge piers have been carried out using open-channel flow conditions. The number of studies on the flow field around both bridge abutments and bridge pier under ice-covered condition is very limited. Zabilansky et al. [32] performed a series of flume experiments under smooth and rough ice cover conditions and found that the maximum velocity for rough ice cover was 20% greater than for smooth ice cover. This statement was confirmed by Muste et al. [33] who found that the measured maximum velocity under smooth cover is located roughly at  $0.8y_0$ , while maximum velocity under rough cover is approximately located at  $0.6y_0$ , where  $y_0$  represents the approaching flow depth. **Figure 1** illustrates the impact of ice cover around the bridge foundation of the Confederation Bridge located in Prince Edward Island in 2015.

*Objective:* The second objective of this study is to investigate the velocity distribution under ice-covered flow conditions and discuss on their difference with that of the open-channel flow conditions to gain a better understanding of the flow field and velocity distribution around bridge piers under different flow covers.

#### 1.4 The incipient motion of sediment particles under ice-covered flow condition

One of the main features of the local scour phenomenon which helps river engineers to have a better perception of the deformation of riverbed is the ability to predict the incipient motion of bed material. Furthermore, the development of an armor layer in the scour hole around bridge piers is associated with incipient motion of sediment particles. Bed armoring process typically occurs in streams with nonuniform bed materials. This phenomenon occurs mainly due to selective erosion process in which the bed shear stress of finer sediment particles exceeds the associated critical shear stress for movement. Consequently, finer sediment particles are transported and leave coarser grains behind. Through this process, the coarser grains get more exposed to the flow, while the remaining finer grains get hidden among larger ones [34]. Armor layer is also partially due to the reduced exposure of the flow with those sediments inside the scour hole zone [29]. For the same bed sediments, Dey and Raikar [35] found that the scour depth around bridge piers with an armor layer is less than that without armor layer. Froehlich [36] stated that the thickness of the natural armor layer is up to one to three times the particle grain size of armor layer. Raudkivi and Ettema [37] found that due to the local flow structure around a pier, local scour may either develop through the armor layer and into the finer, more erodible sediment, or it may trigger a more extensive localized type of scour caused by the erosion of the armor layer itself. Sui et al. [29] studied



**Figure 1.**  
*The ice cover around bridge piers (the confederation bridge, Prince Edward Island, 2015).*

clear-water scour around semielliptical abutments with armored beds. The results showed that for any bed material having the same grain size, with the increase in the particle size of armor layer, scour depth will decrease.

The determination of the critical condition for incipient motion of sediment and the sediment transport rate are highly crucial. To study the incipient motion of sediment particle, the Shields diagram [38] is widely accepted. It is a graph of boundary shear stress nondimensionalized by the submerged specific weight and the mean size of the sediment particle which is called the Shields parameter, Shields criterion, Shields number, or dimensionless shear stress ( $\tau_c^*$ ) against the boundary Reynolds number ( $Re^*$ ). According to Shields [38], the critical conditions in which sediment is on the verge of becoming entrained can be determined by relating the critical Shields value ( $\tau_c^*$ ) and the shear Reynolds number ( $Re^*$ ). The boundary shear Reynolds number is defined as follows:

$$Re^* = \frac{U^* D_i}{\nu} \quad (1)$$

where  $D_i$  is the grain size diameter,  $\nu$  is the kinetic viscosity of fluid, and  $U^*$  is shear velocity.

In this study, since the applied bed materials are composed of nonuniform natural sediment, the particle grain size is not constant. Therefore, the median grain size of nonuniform sand ( $D_{50}$ ) is used to represent the particle size for calculating the critical shear Reynolds number. The shear velocity ( $U^*$ ) in Eq. (1) can be determined as follows:

$$U^* = \sqrt{gRS} \quad (2)$$

where  $S$  is the channel slope,  $R$  is the hydraulic radius, and  $g$  is the gravitational acceleration. The dimensionless shear stress is used to calculate the initiation of sediment motion in a fluid flow. The critical dimensionless shear stress ( $\tau_c^*$ ) is defined as follows:

$$\tau_c^* = \frac{\rho U_c^{*2}}{(\rho_s - \rho)gD_{50}} = \frac{\tau}{(\rho_s - \rho)gD_{50}} \quad (3)$$

in which  $\rho_s$  and  $\rho$  are the mass density of sediment and water, respectively, and  $U_c^*$  is the critical shear velocity ( $U_c^*$ ) that initializes the motion of the particles. In general, the theoretical prediction of the critical condition for incipient motion is based on a force or momentum balance between the destabilizing hydrodynamic drag ( $F_D$ ) and lift forces ( $F_L$ ) against the resisting gravitational ( $W$ ) and frictional forces ( $F_R$ ). Sediment particle will be moved if the applied forces overcome the resistance force. At the threshold of movement, the applied forces are just in balance with the resisting force. In other words, a sediment particle is at a state of incipient motion when the following conditions have been satisfied:

$$\begin{aligned} F_D &= F_R \sin \alpha \\ W &= F_L + F_R \cos \alpha \end{aligned} \quad (4)$$

in which  $\alpha$  is the scour angle. The submerged weight of the particle can be given by

$$W = \frac{\pi d^3}{6} (\rho_s - \rho)g \quad (5)$$

where  $\rho$  and  $\rho_s$  are the density of water and sediment, respectively, and  $d$  is the sediment size in the armor layer. Apart from geometric details such as bed slope, particle exposure, and pocket geometry, accurate prediction of incipient motion requires precise knowledge of the hydrodynamic drag ( $F_D$ ) and lift forces ( $F_L$ ) acting on the particle. By using Yang's criteria [39] for incipient motion, the drag force can be expressed as

$$F_D = C_D \frac{\pi d^2 \rho}{4} \frac{V_s^2}{2} \quad (6)$$

where  $C_D$  is the drag coefficient at velocity  $V_s$  and  $V_s$  is the local velocity at a distance "s" above the bed. The lift force acting on the particle can be obtained as

$$F_L = C_L \frac{\pi d^2 \rho}{4} \frac{V_s^2}{2} \quad (7)$$

where  $C_L$  is the lift coefficient at velocity  $V_s$ . Meyer-Peter and Müller [40] proposed the following equation to calculate the sediment size in the armor layer:

$$d = \frac{SH}{K_1 \left( n/D_{90}^{1/6} \right)^{3/2}} \quad (8)$$

in which  $d$  is the size of sediment in the armor layer,  $S$  is the slope of the channel,  $H$  is the depth of mean flow,  $K_1$  is the constant number equal to 0.058 when  $H$  is in m,  $D_{90}$  is the bed material size where 90% of the material is finer, and  $n$  is the roughness of the channel bottom or Manning's roughness. To calculate the critical bed shear velocity in Eq. (3), Eq. (9) which is developed based on the "law of wall method" can be used. The law of wall method was originally proposed by Von Kármán [41] and supposed that the velocity profile in the lower portion of an open channel flow has a logarithmic distribution [42]:

$$U_c^* = \frac{\bar{u} k}{Ln(z/z_0)} \quad (9)$$

in which  $\bar{u}$  is the average cross-sectional flow velocity,  $k$  is the Von Kármán's constant which is supposed to be 0.4,  $z$  represents the distance from channel bed which is supposed to be depth of water, and  $z_0$  is the roughness height which is supposed to be  $D_{50}$  of the sediment particles. Due to the presence of  $U_c^*$  in both axes of the Shields diagram, Madsen and Grant [43] introduced a new variable rather than the shear Reynolds number in the horizontal axis of the Shields diagram which is called the sediment-fluid parameter ( $S^*$ ). The sediment-fluid parameter ( $S^*$ ) can be calculated from the following equation:

$$S^* = \frac{D_{50}}{4\nu} \sqrt{(SG - 1)gD_{50}} \quad (10)$$

in which  $SG$  represents the specific weight of sediment.

The transportation process of uniform sediment has been broadly studied, and the mechanism of sediment transport has been well discussed [44]. However, the existing knowledge for estimating the nonuniform sediment transport is still limited. Moreover, results of laboratory experiments using uniform sediment is not an appropriate representative of natural river systems since bed materials in natural riverbeds are nonuniform and composed of sediment particles with different grain

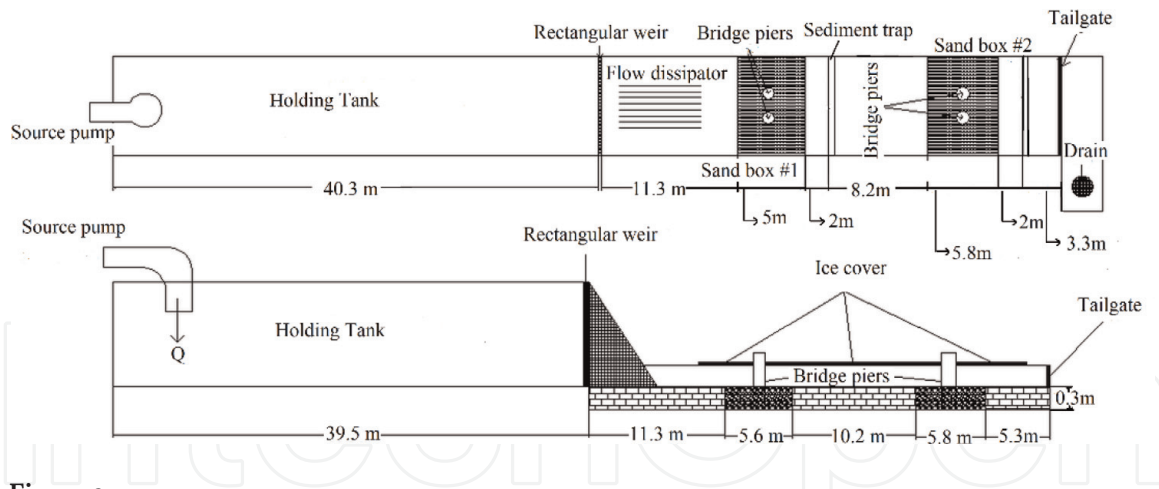


**Figure 2.**  
 Plan view and side view of the experimental flume.

sizes. During the movement process of nonuniform sediment, the coarse grains are easier to be entrained than the same particle size of uniform sediment, because they have higher probabilities to be exposed to the flow. On the other hand, a finer grain tends to be hidden beneath the coarse grains. One of the earliest researches regarding the calculation of the bed load transport rate in a nonuniform riverbed was done by Einstein [45]. In his proposed bed-load function, he used a comprehensive hiding factor to represent the interaction effects between the coarse particles and the fine particles. Ever since, several researchers have developed formulae to determine the incipient motion of nonuniform sediment mixtures [46, 47]. For instance, Xu et al. [47] studied the incipient velocity of nonuniform sediment. As pointed out by Xu et al. [47], the incipient velocity for the coarse particles of the nonuniform sediment is less than that for same particle size of uniform sediment, and the incipient velocity for the finer particles of the nonuniform sediment is greater than that for the same particle size of uniform sediment (**Figure 2**).

The number of studies on the incipient motion of sediment particles is even more limited under ice-covered flow conditions. Since ice cover imposes an additional solid boundary on the flow, the incipient motion of sediment under ice-covered flow condition is different from that under open-channel flow condition. Wang et al. [24] studied the impacts of flow velocity and water depth on the incipient motion of bed material under ice-covered condition. It was found that the deeper the flow depth under ice cover, the higher the flow velocity needed for the incipient motion of bed material.

*Objective:* The third objective of this study is to investigate the features of incipient motion of three nonuniform sediments under ice-covered conditions and to identify the effects of flow roughness caused by ice cover on the incipient motion of nonuniform sediment based on a series of large-scale flume experiments.

## 2. Experimental setup and measurement

Experiments were conducted in a large-scale flume at the Quesnel River Research Centre at the University of Northern British Columbia. The flume was 38.2 m long, 2 m wide, and 1.3 m deep. To generate a higher velocity in the long flume, the relative slope of 0.2% was used. **Figure 3** shows a plan view and a side view of the experimental flume. A holding tank with a volume of 90 m<sup>3</sup> was located in the upstream to maintain a constant flow rate during experimental runs. Three valves were connected to create different velocities. At the end of the flume, water

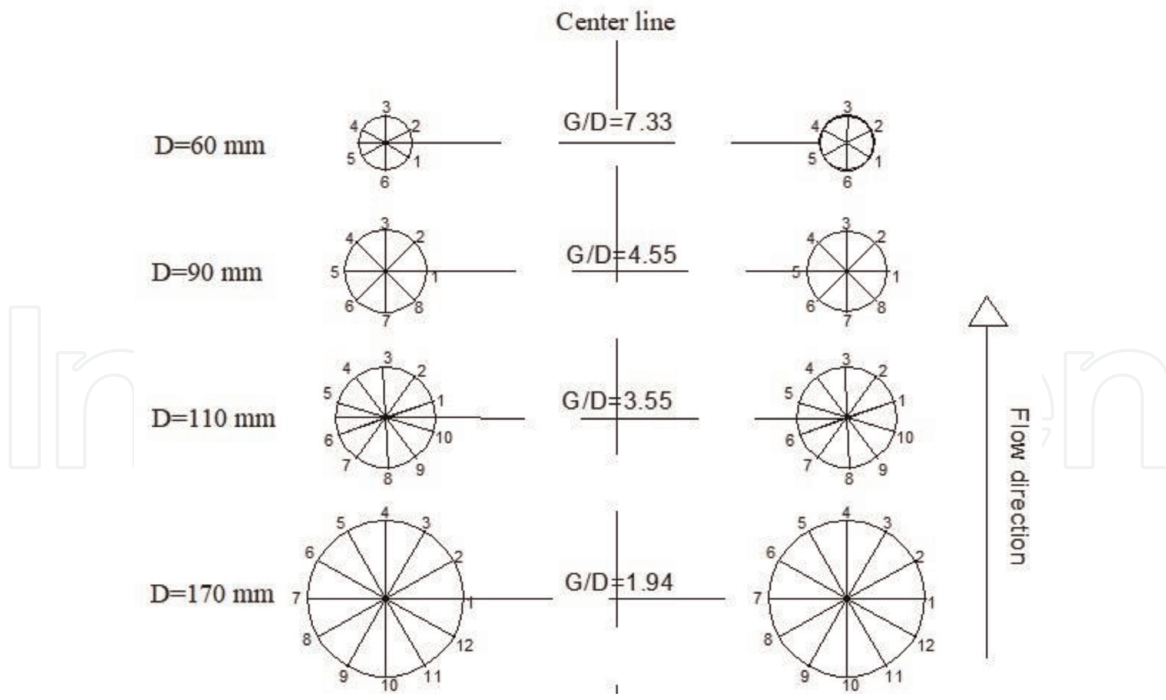


**Figure 3.**  
The spacing ratio and measuring points around the circular bridge piers.

can be recirculated back into the holding tank. Two sandboxes were constructed with a depth of 0.30 m. The distance between the two sandboxes was 10.2 m to avoid potential disturbance. The first and the second sand box were 5.6 and 5.8 m in length, respectively. In each sand box, a pair of bridge piers was positioned in the middle of the sand box. In the present experiments, three types of nonuniform sediments with median grain sizes of 0.50, 0.47, and 0.58 mm were used. **Figure 4** shows the sediment distribution curve of the three existing sediments. This selection of sediments was based upon the fact that the masonry ( $D_{50} = 0.47$  mm), concrete ( $D_{50} = 0.58$  mm), and bedding sand ( $D_{50} = 0.50$  mm) were the three most common sands in the surrounding areas [48]. Four pairs of cylindrical bridge piers with diameters of 60, 90, 110, and 170 mm were used as shown in **Figure 5**. Each pier was offset from the centerline by 0.25 m. The bridge pier spacing ranges from 1.94 to 7.33 relative to  $D$ . The level of water surface was maintained by the downstream tailgate. A SonTek two-dimensional (2D) Flow Meter was mounted in front

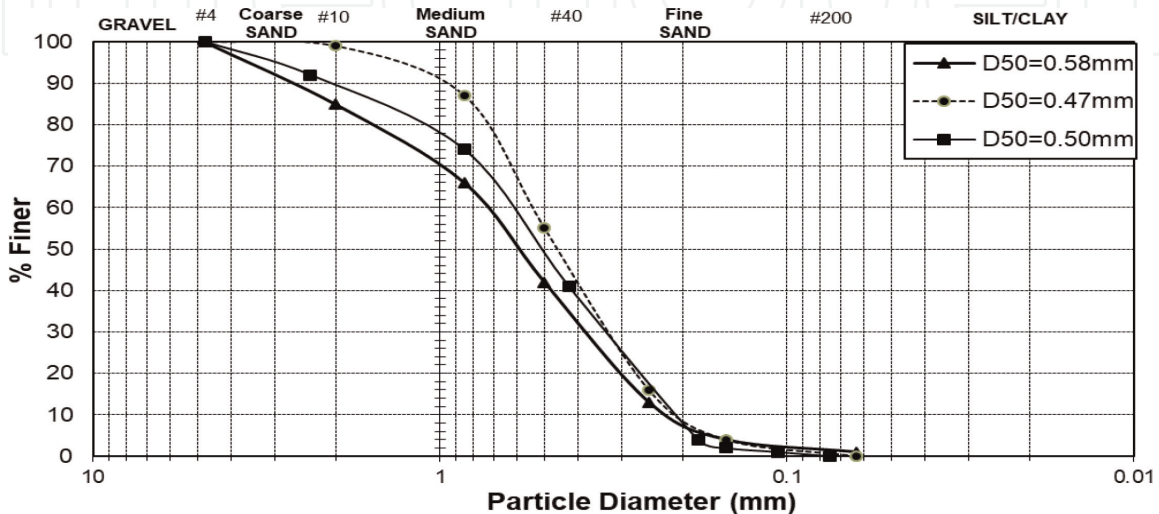


**Figure 4.**  
Distribution curves of the three nonuniform sediments.

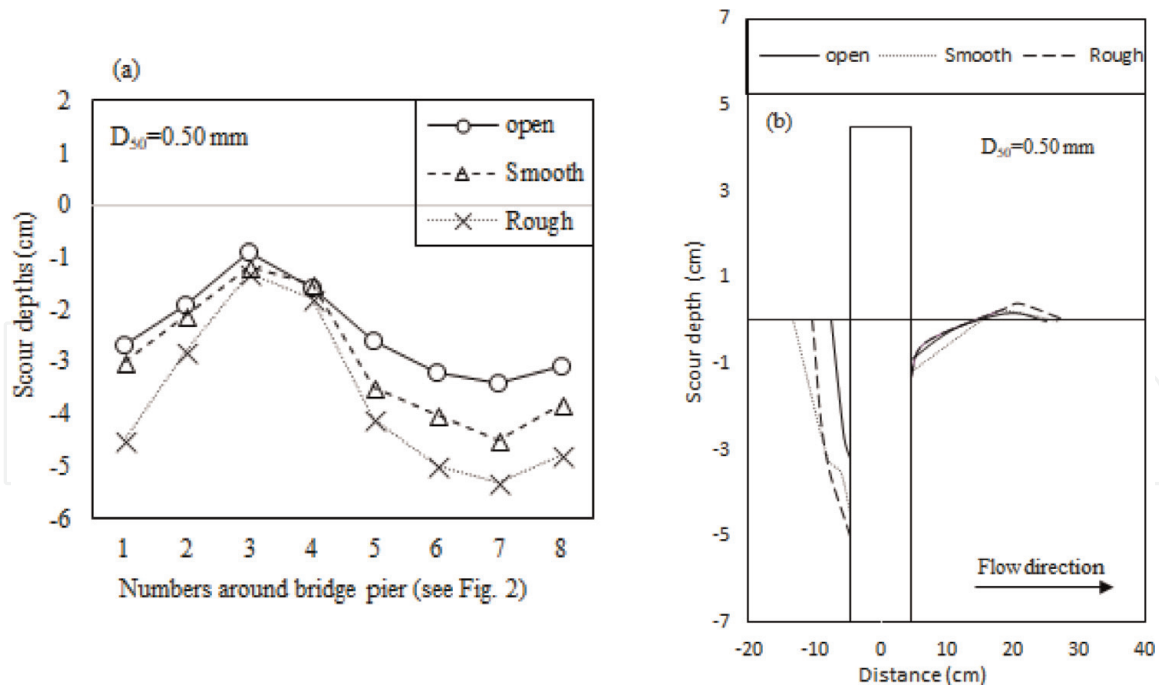


**Figure 5.**  
 (a) Variation of scour depth around the 9-cm piers for  $D_{50} = 0.50$  mm type under open-channel, smooth-covered, and rough-covered flow conditions. (b) Scour and deposition patterns at the pier face of the 9-cm piers under open-channel, smooth-covered, and rough-covered flow conditions ( $D_{50} = 0.50$  mm).

of the first sand box to measure water flow depth and water flow velocity. Besides, the level of water depth was manually rechecked by a staff gauge which was placed in the middle of each sand box. The three-dimensional scour hole velocity fields were measured using a 10-MHz acoustic Doppler velocimeter (ADV). The ADV is an instrument used to measure three-dimensional (3D) flow velocity with high precision. It is applicable to different aspects of environmental issues [49]. In order to simulate the conditions of flow under ice cover, floatable styrofoam panels were used, and they had covered the entire surface of the flume. In the present study, two types of ice cover were used, namely, smooth cover and rough cover. The smooth cover was just the smooth surface of the original Styrofoam panels without any modification, while the rough cover was made by attaching small Styrofoam cubes with dimensions of  $250 \times 25 \times 25$  mm to the bottom of the smooth cover. The styrofoam cubes were spaced 35 mm apart, and they were attached to the smooth cover by toothpicks. Hains et al. [50] declared that fixed rough ice covers lead to the highest local scour in the vicinity of bridge piers compared to those of floating covers and smoother ice, because the rigid ice cover moves the maximum velocity to be closer to the bed. In total, 108 experiments (36 experiments for each sediment type) were done for each sediment type of those 12 experiments which were done under different flow covers (open-channel, smooth-covered, and rough-covered conditions). In terms of measuring the development of the scour holes over the course of time, scour around bridge piers was meticulously recorded hourly for any variation in the scour depths. It was observed that after about a period of 6 h, scour hole reached to the equilibrium state and no significant changes were observed in scour depth. However, the running experimental time for the present experiments was 24 h to be compatible with the experimental results of Wu et al. [51].

After 24 h, the flume was gradually drained off, and the scour and deposition pattern around the piers were recorded. The outside perimeter of each bridge pier was labeled and divided into equal sections to accurately draw scour hole contours. The measurement of the scour hole was subject to an error of  $\pm 0.3$  mm.

As far as the kinematic and dynamic similarity are concerned, the Froude number ( $Fr$ ), which is a measure of the ratio of the inertia force to gravity force, is considered for this type of similitude [53]. In the present study, types of flow for all the experimental runs were turbulent ( $Re_b > 4000$ ) and subcritical ( $Fr < 1$ ) which is the most common case in majority of the rivers.

One of the issues associated with settlement of bridge pier is blockage which reduced the flow cross section. Of note, the blockage refers to the impact of the side walls of a test section on the local scour depth. Chiew [54] declared that if the ratio of pier size to channel width is less than 10% ( $D/W < 10\%$ ), the sidewalls will have no substantial influence on flow characteristics and the scour profile accordingly. Significant sidewall effects in terms of scour happening near to the sidewall are available in the research done by Sheppard et al. [55] in which the blockage ratio is 15%.

In the present study, the ratio of pier size to channel width ( $D/W$ ) ranges from 6 to 17%. The 170-mm pier whose blockage ratio exceeds 15% was located in the second sand box to minimize the impact of the blockage ratio. As suggested by Ettema [56], when  $D/D_{50} < 25$ , individual grains are relatively large compared to the scour hole, and entrainment of sediment particles is hindered because the porous bed dissipates some of the energy of the downflow. Ettema [56], Breusers and Raudkivi [57] confirmed that, when  $D/D_{50} > 25$ , the particle size does not affect the relative scour depth. However, Yanmaz [58] declared that the particle size does not affect the relative scour depth when  $D/D_{50} > 50$ . In the present study, the ratio of  $D/D_{50}$  falls between 206.9 and 723.4 to avoid any impact from  $D/D_{50}$  (the relative pier size) on scour depth.

### 3. Results and analysis

#### 3.1 Scour patterns and deposition patterns

**Figure 5a** shows scour depths around the 90-mm piers, and **Figure 5b** shows the scour and deposition patterns at the pier face for the 90-mm piers under different boundary conditions for  $D_{50} = 0.50$  mm. The results show that the maximum scour depths occurred at the upstream, front face of the bridge piers, regardless of the roughness of ice cover and the grain size of sediment. Under ice-covered flow conditions, the strength of this downflow jet is increased. The eroded sand particles are moved by the joint action of accelerating flow and the horseshoe vortex [52]. Melville and Coleman [59] declared that the wake vortex system which develops behind the pier carries the sediment to the downstream side of the pier. However, wake vortices are not as sturdy as the horseshoe vortices and, consequently, are not capable of carrying the same amount of sediment load as of the horseshoe vortex. As a result, sediment deposition ridge develops downstream of piers in the shape of a deposition mound, as clearly shown in **Figure 5b**. The scour pattern around the 110-mm bridge pier under the highest flow discharge viewed from the top for  $D_{50} = 0.47$  mm was mapped into Surfer 13 plotting software (Golden Software, 1999) as shown in **Figure 6a-c** for open, smooth, and rough flow cover, respectively. According to **Figure 6**, the deepest location of scour depth around the pier is clearly at the face of bridge pier, and the location of deposition ridge is downstream of the pier which is densest and most widely spread for the rough ice-covered flow condition. The same pattern was observed for the other bridge piers regardless of sediment type and bridge pier diameter. It was experimentally noted by Qadar [60] that the maximum value of scour depth should certainly be a function of the initial vortex strength. Therefore, the deepest scour depth, which is the result of a stronger

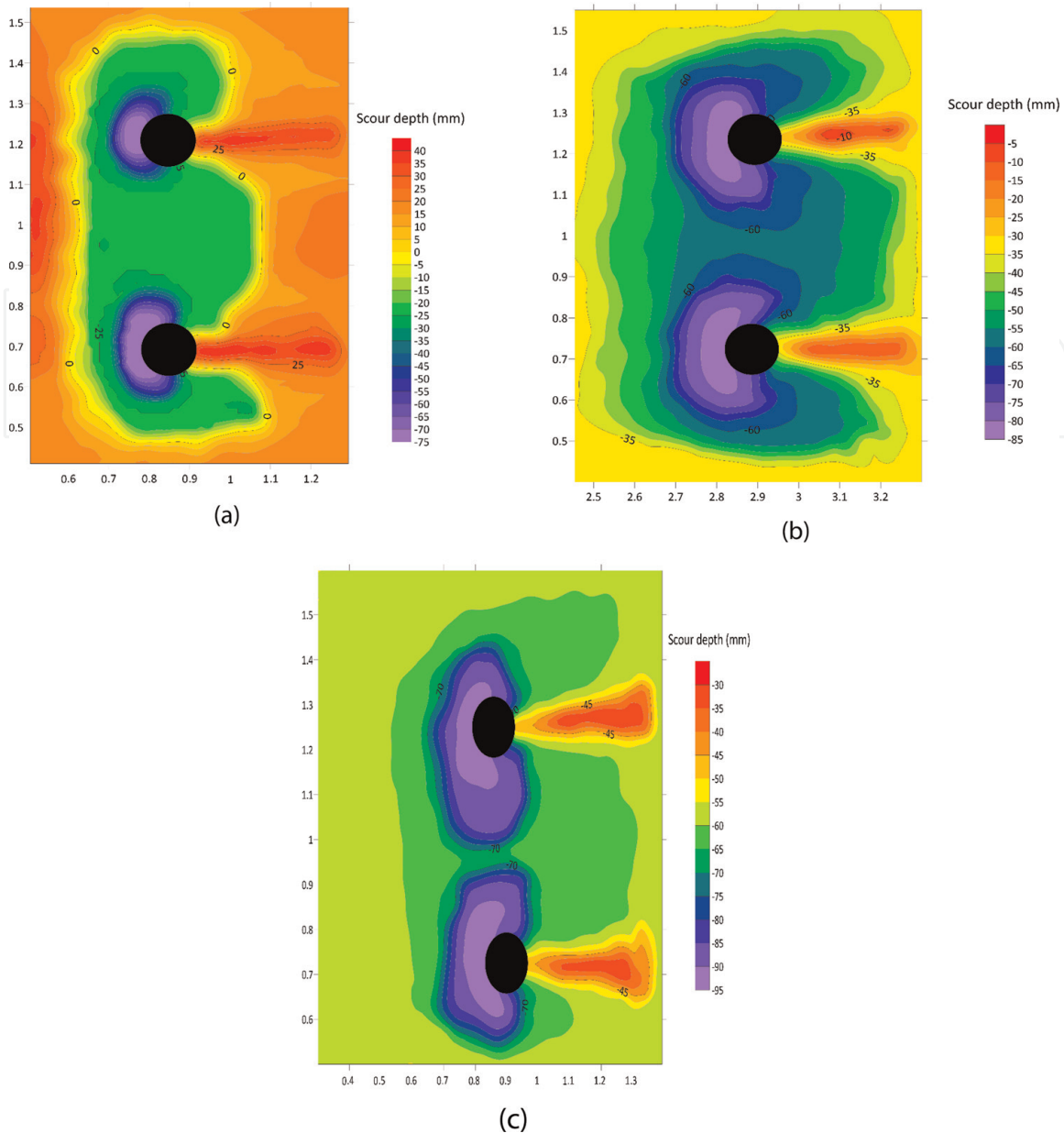


**Figure 6.**

(a) Scour pattern around the 110-mm bridge pier for  $D_{50} = 0.470$  mm type under open for the highest flow discharge. (b) Scour pattern around the 110-mm bridge pier for  $D_{50} = 0.470$  mm type under smooth for the highest flow discharge. (c) Scour patterns around the 110-mm bridge pier for  $D_{50} = 0.470$  mm type under rough for the highest flow discharge.

vortex, should occur under the highest approach velocity and rougher ice cover type as observed in these experiments.

It is obvious that the maximum scour depth and maximum deposition height under the rough-covered flow are visibly greater than that of the open-channel flow. The scour depth contours show that the horseshoe vortex, which is the main cause for the local scour, must have happened nearer to the channel bed which resulted in a greater scour depth under the rough ice-covered flow conditions. The results also show that more sediment deposition develops at the downstream side of bridge piers under the rough ice-covered flow conditions and the deposition mound is more widespread than those under open-channel flow (Figure 6). The reason might be attributable to the velocity distribution variations and larger strength of the horseshoe vortex adjacent to the bed surface under ice-covered conditions. Regardless of sediment type and pier size, similar scour/deposition forms have been observed for other bridge piers. The elevation of the deposition mound downstream

of the bridge piers rests on the depth of the scour hole upstream of the bridge pier along with the interaction between horseshoe vortices and wake vortices. The results specify that higher values of velocity of approaching flow under rough-covered flow conditions result in larger deposition mound at the downstream of the bridge pier.

### 3.2 Effect of pier spacing distance on the scour patterns

**Figure 7** shows the ratio of pier spacing distance to pier diameter ( $G/D$ , termed as bridge pier spacing ratio) against the ratio of the maximum scour depth to the depth of approaching flow ( $y_{max}/y_0$ , termed as relative  $MSD$ ) for  $D_{50} = 0.50$  mm. In **Figure 7**,  $G/D$  ranges from 3.54 to 7.33, and the Froude number ranges from 0.072 to 0.270. In the present study, due to the longitudinal slope of the bed channel and the dissipation of momentum of the flow attributable to friction, the Froude number in the first sand box was higher than that in the second sand box. In the first sand box, either the 110-mm-diameter piers or the 90-mm-diameter piers were placed, and in the second sand box, either the 170-mm-diameter piers or the 60-mm-diameter piers were positioned. According to **Figure 7**, the relative  $MSD$  declines with increase in  $G/D$ . Further, for the same bridge pier spacing ratio ( $G/D$ ) and for the same sediment, the relative  $MSD$  under the rough-covered flow reaches the highest, and the relative  $MSD$  under open-channel flow conditions is the lowest. **Figure 8** displays the variations of the pier Reynold number ( $Re_b$ ) with the pier spacing ratio ( $G/D$ ) for  $D_{50} = 0.50$  mm. The pier Reynolds number is defined as follows:

$$Re_b = \frac{UD}{\nu} \quad (11)$$

where  $U$  is the average velocity of the approaching flow,  $\nu$  is the kinematic viscosity, and  $D$  is the diameter of the bridge pier. The pier Reynold number ( $Re_b$ ) declines with increases in  $G/D$  as shown in **Figure 8**. Hopkins et al. [61] specified that the strength of the horseshoe vortex is a function of the pier Reynolds number

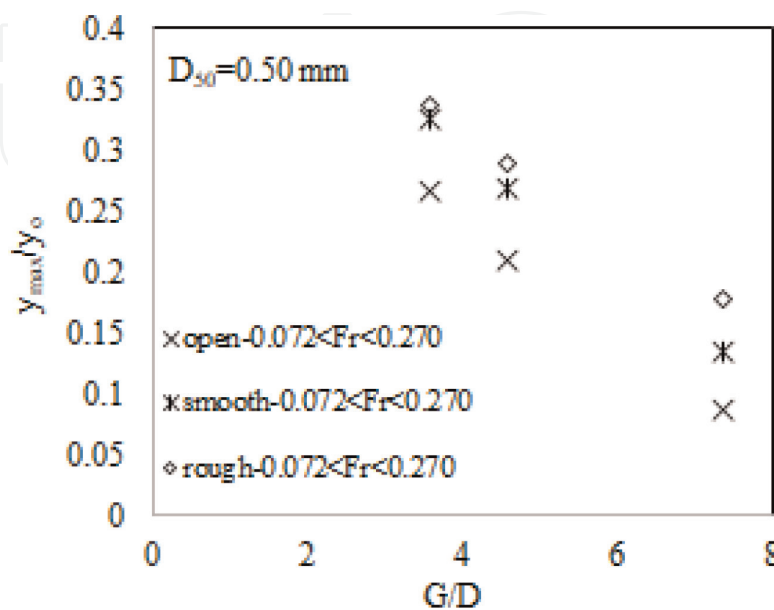


**Figure 7.** Relative  $MSD$  ( $y_{max}/y_0$ ) against pier spacing ( $G/D$ ) under open-channel, smooth-covered, and rough-covered flow conditions ( $D_{50} = 0.50$  mm).

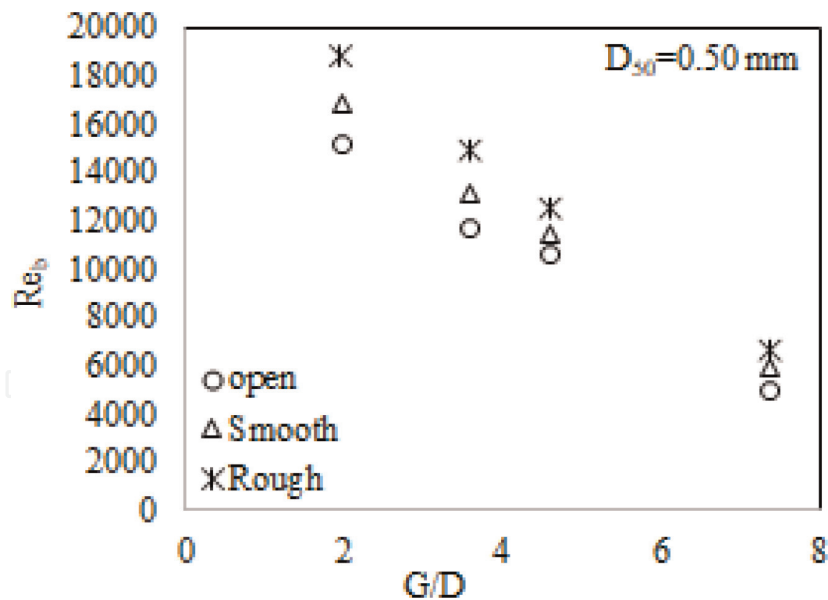


**Figure 8.**  
 Variation of pier spacing ( $G/D$ ) with respect to pier Reynolds number ( $Re_b$ ).

( $Re_b$ ). Hence, it can be determined that the strength of horseshoe vortices, which is a function of  $Re_b$ , declines with increase in the pier spacing ratio. So, the larger the pier spacing ( $G$ ), the smaller the pier size ( $D$ ) and the weaker the horseshoe vortices around bridge piers, which results in shallower scour depths around the bridge piers. Based on **Figure 8**, under the same flow velocity and flow depth, the lowest pier Reynolds number ( $Re_b$ ) happened under the open-channel flow conditions, and the maximum pier Reynolds number ( $Re_b$ ) happened under rough ice-covered flow condition. Though with an increase in the pier spacing ratio, the pier Reynolds number under rough ice-covered flow conditions moves nearer to bed than those of the smooth-covered and open-channel flow conditions, indicating that the impact of ice cover on pier Reynolds number lessens as the pier spacing distance rises.

### 3.3 Velocity profile under ice cover

Scour hole velocity profiles were measured for approaching flow depths ranging from 0.18 to 0.28 m. For shallow flow depths (less than 0.10 m), scour hole velocity measurements were unable to carry out due to limitations of the ADV in shallow water. Since the ADV measuring volume is located 0.10 m from the probe head, the velocity profile does not fully cover up to the water surface. In order to gain an entire velocity profile, it is recommended to use Sontek's 16 MHz micro ADV whose flow volume is measured 0.05 m from the probe head. Of note, since the ADV functions on the principal of a Doppler shift, the velocity values very close to the bed are representative of both sediment and water mixture velocities. Even though clear-water scour was achieved, it is impossible to achieve water velocity, only measurements within 10 mm of the bed. This was also noted by Muste et al. [33]. Velocity measurements were performed 1 h before the end of the experimental run, at which the scour hole was fully developed and stabilized based on the visual observation. Of note, the rate of change of scouring around the bridge pier was too small as it gets closer to the equilibrium scour depth (24 h). The ADV measures velocity in x, y, and z directions. Therefore, the streamwise velocity component ( $U_x$ ) is the component of scour hole velocity in the direction of the flow, the spanwise velocity component ( $U_y$ ) is the component of scour hole velocity in the lateral direction, and the velocity component ( $U_z$ ) is the component of scour hole

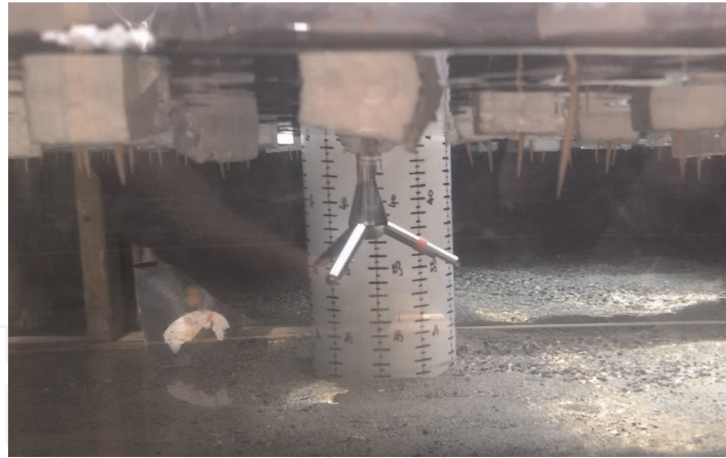


**Figure 9.**  
The ADV measurement around the bridge piers under rough ice-covered condition.

velocity in the vertical direction. **Figure 9** illustrates a view of velocity measurement by ADV under rough ice-covered flow conditions. **Figure 10** shows just  $U_x$  scour hole velocity component profile at the upstream face of the 60-mm pier for  $D_{50} = 0.47$  mm under both ice-covered and open-channel flow conditions for the lowest discharge. Since the location of maximum flow velocity was important, only  $U_x$  is shown in **Figure 11**. In order to be able to generalize the velocity profiles and to compare different velocity profiles under different flow conditions, the depth of flow on the vertical axis has been nondimensionalized by ratio of vertical distance of the location of ADV measurement from bed ( $z$ ) to the approaching flow depth ( $y_0$ ). The streamwise scour hole velocity component ( $U_x$ ) is also

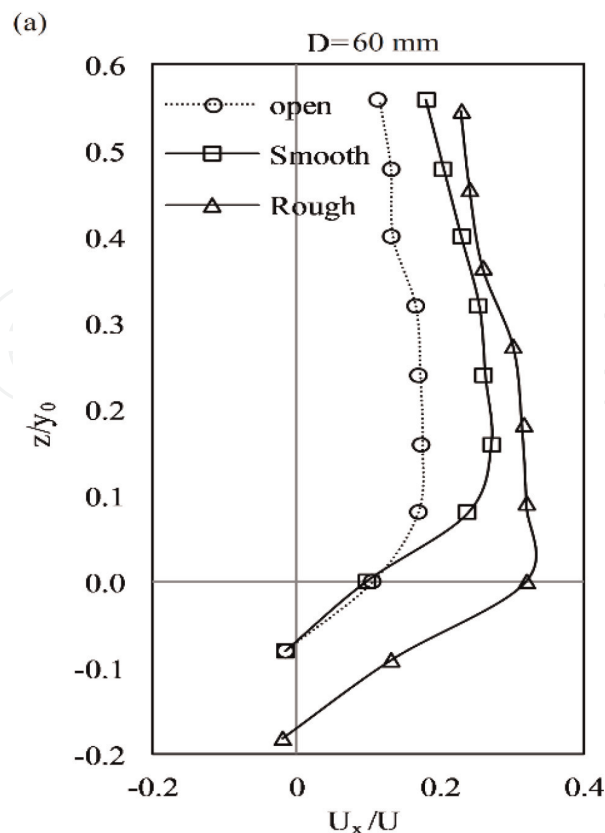


**Figure 10.**  
Scour hole velocity profiles for the streamwise ( $U_x$ ) velocity component under open, smooth, and rough ice cover for 60-mm bridge pier under  $D_{50} = 0.47$  mm for the lowest discharge.

nondimensionalized divided by the approaching flow velocity ( $U$ ). Of note, a SonTek incorporated 2D Flow Meter was installed at the upstream of the first sand box to measure flow velocities and water depth. Results showed that, for the streamwise velocity, distribution is a reverse C-shaped profile which begins from the scour hole up to the water surface. The same pattern was also reported by Hirshfield [48]. In terms of velocity magnitude, the streamwise velocity in the scour hole under rough-covered condition is generally greater than those under both smooth-covered and open flow conditions. Regardless of the cover conditions of the flow, the magnitude of velocity is the least in the scour hole. Also, the values of the velocity component are mostly negative within the scour hole which is an indication of the reversal flow happening due to the presence of the horseshoe vortex which is strongest at the pier face. On the other hand, the location of the maximum velocity is closer to the bed under rough-covered flow condition than that under smooth-covered flow condition. This is in good agreement with the findings of Wang et al. [24].

### 3.4 Shear stress analysis

#### 3.4.1 Shear stress vs. sediment-fluid parameter for the incipient motion of sediment

To the authors' knowledge, shear stress against sediment-fluid parameter for the incipient motion of sediment under ice-covered flow conditions has not been studied before. This information will give a better insight to the hydraulic engineers in terms of sediment incipient motion under ice-covered condition. In **Figure 11** the relationship between  $[S^*(U/U^*)]$  and the dimensionless shear stress ( $\tau^*$ ) is given for channel bed with three different sands with median grain sizes of  $D_{50} = 0.47, 0.50,$  and  $0.58$  mm, respectively. Of note,  $U$  is the mean velocity of approaching flow (m/s),  $U^*$  is the shear velocity (m/s), and  $S^*$  is the sediment-fluid parameter. For each type of the sediment, the sediment-fluid parameter ( $S^*$ ) is unique, and with the increase in  $[S^*(U/U^*)]$ , the dimensionless shear stress increases correspondingly. Also, for all three sands, the larger the  $[S^*(U/U^*)]$ , the greater the dimensionless shear stress for the incipient motion of bed material. For the same  $[S^*(U/U^*)]$ , the finer the sediment, the higher the dimensionless shear stress.

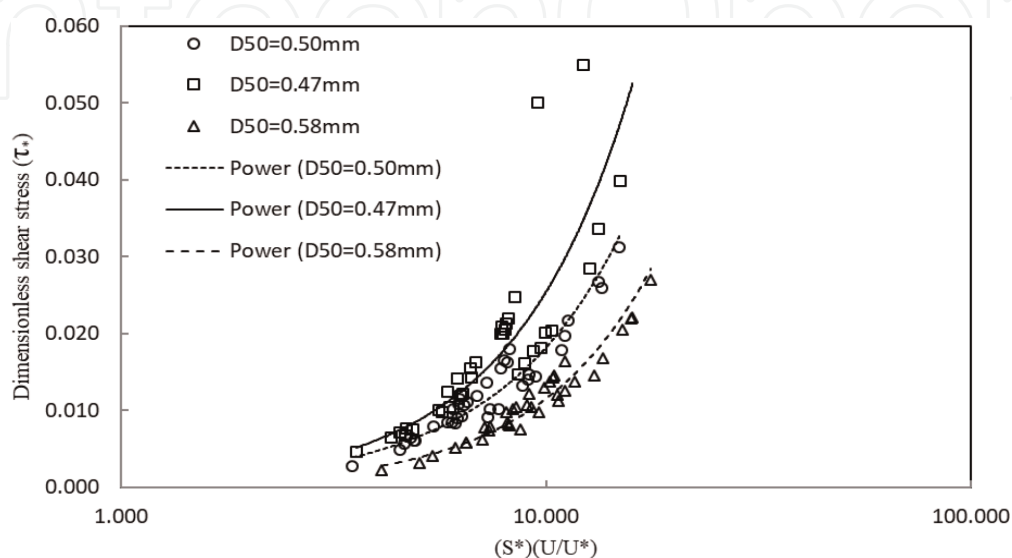


**Figure 11.**  
Dimensionless shear stress ( $\tau^*$ ) vs.  $S^*(U/U^*)$ .

### 3.4.2 Dimensionless shear stress ( $\tau^*$ ) vs. shear Reynolds number ( $Re^*$ ) for the incipient motion of sediment

The relationship between the dimensionless shear Reynolds number and the dimensionless shear stress for the incipient motion of the coarsest sediment ( $D_{50} = 0.58 \text{ mm}$ ) and that of the finest sediment ( $D_{50} = 0.47 \text{ mm}$ ) under both open flow condition and rough ice-covered flow condition has been shown in **Figure 12**. From **Figure 12**, the following observations can be noted:

1. With increase in the dimensionless shear Reynolds number, the dimensionless shear stress increases correspondingly. For all three sands, the larger the dimensionless shear Reynolds number, the greater the dimensionless shear stress for the incipient motion of bed material. However, for the same dimensionless shear stress, the finer sediment has a lower dimensionless shear Reynolds number for the incipient motion of sediment particles.
2. In terms of the impacts of ice cover on the incipient motion of bed material, for the same grain size of sediment, the rough ice cover requires an average lower dimensionless shear stress which implies that the threshold of the dimensionless shear stress for the incipient motion of bed material under rough ice-covered flow condition is lower than that under open flow conditions.

Of note, Wang et al. [24] also studied dimensionless shear stress ( $\tau^*$ ) against shear Reynolds number ( $Re^*$ ) for the incipient motion of sediment under ice-covered condition. Their result showed that for the same sediment grain size, larger values of the shear Reynolds number lead to the larger values of the dimensionless shear stress for incipient motion of bed material. It can also be said that, for the same dimensionless shear stress, the finer sediment particles need a lower value of shear Reynolds number for the incipient motion of sediment.

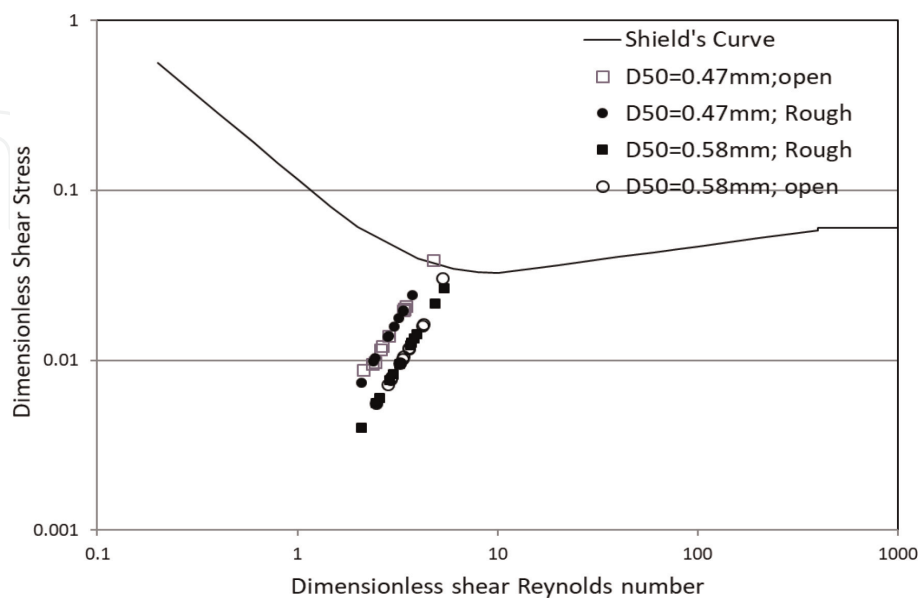


**Figure 12.** Dimensionless shear stress ( $\tau^*$ ) vs. shear Reynolds number ( $Re^*$ ) for the incipient motion of the finest sediment ( $D_{50} = 0.47 \text{ mm}$ ) and the coarsest sediment ( $D_{50} = 0.58 \text{ mm}$ ) under open and rough ice-covered flow conditions.

## 4. Conclusion

In the current study, 108 experiments were done in a large-scale flume with nonuniform sediment to investigate the local scour process, velocity distribution, and incipient motion of sediment particles around four pairs of side-by-side cylindrical bridge piers under open-channel, smooth-covered, and rough-covered flow conditions. The following conclusions can be drawn from the current study:

1. It is found that the presence of ice cover can result in a deeper maximum scour depth than that under open flow condition.
2. The required flow velocity for incipient motion of sediment particles under ice-covered conditions decreases with the increase in the relative roughness coefficient of ice cover.
3. The pier Reynolds number ( $Re_b$ ) declines with the increase in the pier spacing ratio ( $G/D$ ), indicating that the strength of the horseshoe vortices reduces as the spacing distance between the side-by-side piers rises. Further, under the same flow velocity and flow depth, the highest pier Reynolds number ( $Re_b$ ) happened under rough-covered flow conditions, and the lowest pier Reynolds number ( $Re_b$ ) happened under open-channel flow conditions. Moreover, regardless of flow cover, the impact of ice cover on pier Reynolds number diminishes as the pier spacing distance increases. The relative  $MSD$  under open-channel flow conditions is the lowest and maximizes under the rough-covered flow condition for the same bridge pier spacing ratio ( $G/D$ ) and for the same sediment. This indicates that the effect of the pier spacing ratio under the rough ice-covered flow condition is evidently strengthened compared to those under both open-channel and smooth-covered flow conditions.
4. With the increase in the dimensionless shear Reynolds number, the dimensionless shear stress increases correspondingly. For all three sands, the larger the dimensionless shear Reynolds number, the greater the dimensionless shear stress for the incipient motion of bed material. However, for the same dimensionless shear stress, the finer sediment has a lower dimensionless shear Reynolds number for the incipient motion of sediment particles.
5. In terms of the impacts of ice cover on the incipient motion of bed material, for the same grain size of sediment, the rough ice cover requires an average lower dimensionless shear stress which implies that the threshold of the dimensionless shear stress for the incipient motion of bed material under rough ice-covered flow condition is lower than that under open flow conditions.

IntechOpen

**Author details**

Mohammad Reza Namaee<sup>1</sup>, Jueyi Sui<sup>1\*</sup> and Peng Wu<sup>2</sup>

1 University of Northern British Columbia, Prince George, BC, Canada

2 University of Regina, Regina, SK, Canada

\*Address all correspondence to: [jueyi.sui@unbc.ca](mailto:jueyi.sui@unbc.ca)

**IntechOpen**

---

© 2019 The Author(s). Licensee IntechOpen. This chapter is distributed under the terms of the Creative Commons Attribution License (<http://creativecommons.org/licenses/by/3.0>), which permits unrestricted use, distribution, and reproduction in any medium, provided the original work is properly cited. 

## References

- [1] Basson GR. Hydraulics of two-phase flows: Water and sediment. Hydraulic Structure, Equipment and Water Data Acquisition Systems—Volume I. 2009. pp. 123
- [2] Chiew YM, Melville BW. Local scour around bridge piers. *Journal of Hydraulic Research*. 1987;25(1):15-26
- [3] Richardson EV, Davis SR. *Evaluating Scour at Bridges*. Washington, DC: HEC18 FHWA NHI-001, Federal Highway Administration, US Department of Transportation; 2001
- [4] Zhang Q, Zhou XL, Wang JH. Numerical investigation of local scour around three adjacent piles with different arrangements under current. *Ocean Engineering*. 2017;142: 625-638
- [5] Melville BW, Raudkivi AJ. Flow characteristics in local scour at bridge piers. *Journal of Hydraulic Research*. 1977;15(4):373-380
- [6] Briand JL, Hunt BE. Bridge scour & the structural engineer. *Structure Magazine*. 2006:59-61
- [7] Wardhana K, Hadipriono FC. Analysis of recent bridge failures in the United States. *Journal of Performance of Constructed Facilities*. 2003;17(3): 144-150
- [8] Raudkivi AJ. Functional trends of scour at bridge piers. *Journal of Hydraulic Engineering*. 1986;112(1):1-13
- [9] Mendoza-Cabrales C. Computation of flow past a cylinder mounted on a flat plate. In: *Hydraulic Engineering*; ASCE. 1993. pp. 899–904
- [10] Unger J, Hager WH. Down-flow and horseshoe vortex characteristics of sediment embedded bridge piers. *Experiments in Fluids*. 2007;42(1):1-19
- [11] Muzzammil M, Gangadhariah T. The mean characteristics of horseshoe vortex at a cylindrical pier. *Journal of Hydraulic Research*. 2003;41(3):285-297
- [12] Dou X. Numerical simulation of three-dimensional flow field and local scour at bridge crossings [dissertation]. University of Mississippi; 1997
- [13] Dehghani AA, Esmaili T, Kharaghani S, Pirestani MR. Numerical simulation of scour depth evolution around bridge piers under unsteady flow condition. In: *Water Engineering for a Sustainable Environment*. Vancouver: IAHR; 2009. pp. 5888-5895
- [14] Amini A, Melville BW, Ali TM, Ghazali AH. Clear-water local scour around pile groups in shallow-water flow. *Journal of Hydraulic Engineering*. 2011;138(2):177-185
- [15] Melville BW, Sutherland AJ. Design method for local scour at bridge piers. *Journal of Hydraulic Engineering*. 1988; 114(10):1210-1226
- [16] Richardson EV, Simons DB, Lagasse PF. *River Engineering for Highway Encroachments—Highways in the River Environment*. Washington, DC: Federal Highway Administration, Hydraulic Series No. 6; 2001
- [17] Sheppard DM, Melville B, Demir H. Evaluation of existing equations for local scour at bridge piers. *Journal of Hydraulic Engineering*. 2013;140(1):14-23
- [18] Williams P, Balachandar R, Bolisetti T. Evaluation of local bridge pier scour depth estimation methods. In: *Proceedings of the 24th Canadian Congress of Applied Mechanics (CANCAM)*; Saskatoon, Canada: University of Saskatchewan. 2013
- [19] Ataie-Ashtiani B, Beheshti AA. Experimental investigation of

- clear-water local scour at pile groups. *Journal of Hydraulic Engineering*. 2006; **132**(10):1100-1104
- [20] Hannah CR. Scour at pile groups. In: Research Report No. 28–3. Christchurch, New Zealand: Civil Engineering Department, University of Canterbury; 1978
- [21] Salim M, Jones JS. Scour around exposed pile foundations. In: North American Water and Environment Congress & Destructive Water; ASCE. 1996. pp. 2202-2211
- [22] Hains D, Zabilansky LJ, Weisman RN. An experimental study of ice effects on scour at bridge piers. In: Cold Regions Engineering and Construction Conference and Exp; 16–19 May 2004, Edmonton, Alberta, Canada. 2004
- [23] Ettema R, Zabilansky L. Ice influences on channel stability: Insights from Missouri's fort peck reach. *Journal of Hydraulic Engineering*. 2004; **130**(4): 279-292
- [24] Wang J, Sui J, Karney B. Incipient motion of non-cohesive sediment under ice cover—An experimental study. *Journal of Hydrodynamics*. 2008; **20**(1): 117-124
- [25] Hoque M. Hydraulic analysis of ice-covered river flow [doctoral dissertation]. Concordia University; 2009
- [26] Ackermann NL, Shen HT, Olsson P, Squire VA. Local scour around circular piers under ice covers. In: Ice in the Environment: Proceedings of the 16th IAHR International Symposium on Ice, Dunedin, New Zealand; 2–6 December; Madrid. Spain: International Association of Hydraulic Engineering and Research. 2002
- [27] Batuca D, Dargahi B. Some experimental results on local scour around cylindrical piers for open and covered flow. In: Third International Symposium on River Sedimentation. University of Mississippi; 1986
- [28] Wu P, Balachandar R, Sui J. Local scour around bridge piers under ice-covered conditions. *Journal of Hydraulic Engineering*. 2015; **142**(1):04015038
- [29] Sui J, Wang J, He Y, Krol F. Velocity profiles and incipient motion of frazil particles under ice cover. *International Journal of Sediment Research*. 2010; **25**(1):39-51
- [30] Crance MJ, Frothingham KM. The impact of ice cover roughness on stream hydrology. In: 65 the Eastern Snow Conference, Fairlee (Lake Morey), Vermont. 2008. pp. 149
- [31] Beltaos S. River flow abstraction due to hydraulic storage at freeze-up. *Canadian Journal of Civil Engineering*. 2009; **36**(3):519-523
- [32] Zabilansky LJ, Hains DB, Remus JJ. Increased bed erosion due to ice. In: Cold Regions Engineering 2006: Current Practices in Cold Regions Engineering, Reston, VA: American Society for Civil Engineers. 2006. pp. 1-12
- [33] Muste M, Braileanu F, Ettema R. Flow and sediment transport measurements in a simulated ice-covered channel. *Water Resources Research*. 2000; **36**(9):2711-2720
- [34] Mao L, Cooper J, Frostick L. Grain size and topographical differences between static and mobile armour layers. *Earth Surface Processes and Landforms*. 2011; **36**(10):1321-1334
- [35] Dey S, Raikar R. Clear-water scour at piers in sand beds with an armor layer of gravels. *Journal of Hydraulic Engineering*. 2007; **133**:703-711
- [36] Froehlich DC. Armor limited clear water construction scour at bridge.

Journal of Hydraulic Engineering,  
ASCE. 1995;**121**:490-493

[37] Raudkivi AJ, Ettema R. Clear-water scour at cylindrical piers. *Journal of Hydraulic Engineering*. 1983;**109**(3): 338-350

[38] Shields A. Anwendung der Aehnlichkeitsmechanik und der Turbulenzforschung auf die Geschiebepbewegung [thesis]. Berlin: Technical University; 1936

[39] Yang CT. Sediment Transport, Theory and Practice. Malabar, Florida: KRIEGER Publishing Company; 2003. pp. 90-140

[40] Meyer-Peter E, Müller R. Formulas for bed-load transport. In: IAHSR 2nd Meeting, Stockholm, appendix 2. IAHR. 1948

[41] Von Kármán T. 1930, Mechanische Aehnlichkeit und turbulenz (Mechanical similarity and turbulence): The International Congress for Applied Mechanics, 3d, Stockholm 1930, Proc., v. 1, p. 85-92

[42] Barenblatt GI, Chorin AJ. Scaling laws and zero viscosity limits for wall-bounded shear flows and for local structure in developed turbulence. *Communications on Pure and Applied Mathematics*. 1997;**50**(4):381-398

[43] Madsen OS, Grant WD. Quantitative description of sediment transport by waves. In: *Coastal Engineering 1976*. 1977. pp. 1092-1112

[44] Aguirre-Pe J, Olivero MIAL, Moncada AT. Particle densimetric Froude number for estimating sediment transport. *Journal of Hydraulic Engineering*. 2003;**129**(6):428-437

[45] Einstein HA. The Bed-Load Function for Sediment Transportation in Open Channel Flows. Vol. 1026. Washington, DC: US Department of Agriculture; 1950

[46] Andrews ED. Entrapment of gravel from naturally sorted riverbed material. *Geological Society of America Bulletin*. 1983;**94**:1225-1231

[47] Xu H, Lu J, Liu X. Nonuniform sediment incipient velocity. *International Journal of Sediment Research*. 2008;**23**(1):69-75

[48] Hirshfield F. The impact of ice conditions on local scour around bridge piers [dissertation]. Prince George, B.C., Canada: Environmental Engineering Program, University of Northern British Columbia; 2015

[49] Cea L, Puertas J, Pena L. Velocity measurements on highly turbulent free surface flow using ADV. *Experiments in Fluids*. 2007;**42**(3):333-348

[50] Hains D, Zabilansky LJ, Weisman RN. An experimental study of ice effects on scour at bridge piers. In: *Cold Regions Engineering and Construction Conference and Expo*; 16–19 May 2004; Edmonton, Alberta, Canada. 2004

[51] Wu P, Hirshfield F, Sui J. Armor layer analysis of local scour around bridge abutment under ice covered condition. *River Research and Applications*. 2014a;**31**(6):736-746

[52] Yang Q. Numerical investigations of scale effects on local scour around a bridge pier [dissertation]. Tallahassee, FL, USA: Florida State University; 2005

[53] Heller V. Scale effects in physical hydraulic engineering models. *Journal of Hydraulic Research*. 2011;**49**(3):293-306

[54] Chiew YM. Local scour at bridge piers [dissertation]. New Zealand: University of Auckland; 1984

[55] Sheppard DM, Odeh M, Glasser T. Large scale clear-water local pier scour experiments. *Journal of Hydraulic Engineering*. 2004;**130**(10):957-963

[56] Ettema R. Scour at bridge piers. In: Report No. 216. New Zealand: Department of Civil Engineering, University of Auckland; 1980

[57] Breusers HNC, Raudkivi AJ. Scouring, Hydraulic Structures Design Manual, No. 2. I.A.H.R., Boca Raton, Florida, United States: Balkema; 1991. 143 pp

[58] Yanmaz AM. Dynamic reliability in bridge pier scouring. Turkish Journal of Engineering and Environmental Sciences. 2002;26(4):367-376

[59] Melville BW, Coleman SE. Bridge Scour. Highlands Ranch, Colo, USA: Water Resources Publications; 2000

[60] Qadar A. The vortex scour mechanism at bridge piers. In: Institution of Civil Engineers, Proceedings, Pt2 (Vol. 71). September 1981

[61] Hopkins GR, Vance RW, Kasraie B. Scour around bridge piers, FHWA-RD-79-103. U.S. Department of Transportation, Federal Highway Administration, Offices of Research and Development, Environmental Division; Washington, D.C.: 1980